Cross-plane Seebeck coefficient in superlattice structures in the miniband conduction regime

D Vashaee Y Zhang

A Shakouri G H. Zeng Y J. Chiu

Cross-plane Seebeck coefficient in superlattice structures in the miniband conduction regime

Abstract

We have studied experimentally and theoretically the cross-plane Seebeck coefficient of short period InGaAs/InAlAs superlattices with doping concentrations ranging from 2x10(18) up to 3x10(19) cm(-3). Measurements are performed with integrated thin film heaters in a wide temperature range of 10-300 K. It was interesting to find out that contrary to the behavior in bulk material the Seebeck coefficient did not decrease monotonically with the doping concentration. We did not observe a sign change in the Seebeck coefficient at dopings where the Fermi energy is just above a miniband. This is a sign that electrons' lateral momentum is conserved in the transport perpendicular to superlattice layers. A preliminary theory of thermoelectric transport in superlattices in the regime of miniband formation has been developed to fit the experimental results.

Cross-plane Seebeck coefficient in superlattice structures in the miniband conduction regime

Daryoosh Vashaee,[1,*] Yan Zhang,[1] Ali Shakouri,[1] Gehong Zeng,[2] and Yi-Jen Chiu[2]
[1]*Jack Baskin School of Engineering, University of California, Santa Cruz, California 95064, USA*
[2]*Electrical and Computer Engineering Department, University of California, Santa Barbara, California 93106, USA*
(Received 11 July 2006; revised manuscript received 18 September 2006; published 9 November 2006)

We have studied experimentally and theoretically the cross-plane Seebeck coefficient of short period InGaAs/InAlAs superlattices with doping concentrations ranging from 2×10^{18} up to 3×10^{19} cm^{-3}. Measurements are performed with integrated thin film heaters in a wide temperature range of 10–300 K. It was interesting to find out that contrary to the behavior in bulk material the Seebeck coefficient did not decrease monotonically with the doping concentration. We did not observe a sign change in the Seebeck coefficient at dopings where the Fermi energy is just above a miniband. This is a sign that electrons' lateral momentum is conserved in the transport perpendicular to superlattice layers. A preliminary theory of thermoelectric transport in superlattices in the regime of miniband formation has been developed to fit the experimental results.

DOI: 10.1103/PhysRevB.74.195315 PACS number(s): 73.50.Lw, 73.63.−b

I. INTRODUCTION

N-type materials have negative Seebeck coefficients. That is because the energy the electrons contribute in transport is distributed mostly above the Fermi level. This can be shown with the following linear transport equations:

$$\sigma = \frac{e^2}{4\pi^3}\int_{-\infty}^{+\infty}\int_{-\infty}^{+\infty}\int_{-\infty}^{+\infty}\tau(k)v_x^2(k)\left(-\frac{\partial f_{eq}}{\partial E}\right)dk_x dk_y dk_z = \int_0^{\infty}\sigma(E)\left(-\frac{\partial f_{eq}}{\partial E}\right)dE, \tag{1}$$

$$S = \frac{1}{eT}\frac{\int_{-\infty}^{+\infty}\int_{-\infty}^{+\infty}\int_{-\infty}^{+\infty}\tau(k)v_x^2(k)(E(k)-E_F)\left(-\frac{\partial f_{eq}}{\partial E}\right)dk_x dk_y dk_z}{\int_{-\infty}^{+\infty}\int_{-\infty}^{+\infty}\int_{-\infty}^{+\infty}\tau(k)v_x^2(k)\left(-\frac{\partial f_{eq}}{\partial E}\right)dk_x dk_y dk_z} = \frac{k_B}{e}\frac{\int_0^{\infty}\sigma(E)\frac{(E-E_F)}{k_BT}\left(-\frac{\partial f_{eq}}{\partial E}\right)dE}{\int_0^{\infty}\sigma(E)\left(-\frac{\partial f_{eq}}{\partial E}\right)dE} \propto \langle E-E_f\rangle. \tag{2}$$

The "differential" conductivity is defined as

$$\sigma(E) = e^2\tau(E)\int\int v_x^2(E,k_y,k_z)dk_y dk_z \cong e^2\tau(E)\bar{v}_x^2(E)\bar{n}(E), \tag{3}$$

where σ and S are the electrical conductivity and the Seebeck coefficient, respectively. $\tau(E)$ is the energy dependent relaxation time, $v_x(E)$ is the average velocity of the carriers with energy between E and $E+dE$ in the direction of current flow, and $n_x(E)$ is the number of electrons in this energy interval. Electrical conductivity is the sum of the contributions of electrons with various energies E [given by the differential conductivity $\sigma(E)$] within the Fermi window factor $\delta f_{eq}/\delta E$. The Fermi window is a direct consequence of the Pauli exclusion principle, and at finite temperatures only electrons near the Fermi surface contribute to the conduction process. In this picture the Seebeck coefficient described in Eq. (2) is the average energy transported by the charge carriers corresponding to a diffusion thermopower. In *N*-type materials this average energy is positive; hence, the Seebeck coefficient is negative. On the other hand, *P*-type materials generally have positive Seebeck coefficients. Thus for the same bias polarity, the *n*-type device cools on the cathode side and heats on the anode, whereas the *p*-type device heats on the cathode and cools on the anode. This is fortunate as it lets us have a configuration of multi *n*- and *p*-type elements connected electrically in series and thermally in parallel. This arrangement has several advantages over the single-element case. It first allows for the removal of the external electrical connection to the cold side of the device and keeps all external connections on the hot side, close to the heat sink. The other main advantage is in reducing the necessary external current bias. A large-area thermoelement (length and width $\gg$ thickness) requires a much larger current than a small-area thermoelement (length and width $\sim$ thickness) to maintain the same temperature difference. By placing many of the small-area thermoelements together, it is still possible to cool an area that is the same size as the large-area thermoelement. Correspondingly, as the individual elements are made smaller, the required current is reduced and the external voltage is increased.

The overall device performance in conventional thermoelectric coolers is given by the dimensionless figure of merit ZT, which has the equation $ZT=S^2\sigma T/\beta$. This equation describes the tradeoffs between the Peltier cooling given by the Seebeck coefficient (S), the Joule heating given by the electrical conductivity (σ), and the heat conduction from the hot to cold junction given by the thermal conductivity (β). ZT should be maximized to reach optimum performance and efficiency. We have recently shown that thick and tall barrier superlattices can improve ZT substantially if the lateral momentum of electrons is not conserved in thermionic emission process.[1,2]

In this paper, we study thermoelectric transport in short period superlattice structures. Strong coupling between neighboring wells produces minibands. We chose an InGaAs/InAlAs superlattice with a high barrier (0.54 eV). We studied the effect of the doping concentration on the cross-plane Seebeck coefficient at various ambient temperatures.

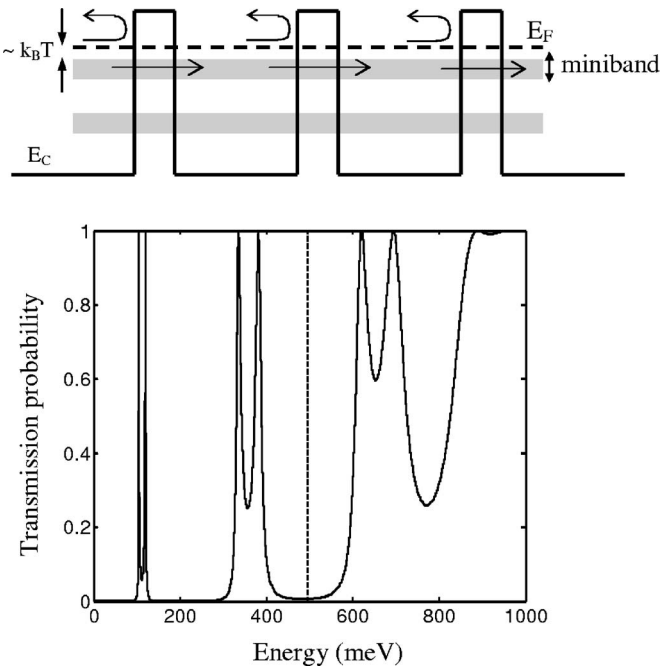

FIG. 1. The above diagram illustrates the concept of manipulating the miniband conduction for electron filtering. Dashed line in transmission probability picture indicates the barrier height of 500 meV (superlattice parameters are listed in Table I).

II. THERMOELECTRIC TRANSPORT IN MINIBAND CONDUCTION REGIME

Figure 1 shows a schematic of the superlattice miniband structure and the corresponding transmission probability for the conduction electrons. If the miniband gap is wide enough and if the Fermi energy is placed approximately k_BT above the miniband, it could be possible to selectively block electrons above the Fermi energy and transmit electrons below the Fermi energy. Consequently, heating and cooling would be reversed compared to a normal n-doped material. Cantrell *et al.*[3] and Larsson *et al.*[4] have also predicted that in a suitable multiple barrier structure, the thermopower may change sign because of quantum transport process. However, they were not concerned about the thermoelectric figure of merit (ZT). Cantrell *et al.*[3] consider the case where the Fermi level (E_F) lies in the neighborhood of a particular subband minimum (E_n). They calculate the corresponding Seebeck coefficient (S) for two cases of $E_F > E_n$ and $E_F < E_n$. They also assume that the differential conductivity, $\sigma(E_F)$, varies linearly on either side of E_n. In this situation, they show that when E_F is close to a subband minimum, S changes sign as T is reduced below ~10 K. Larsson *et al.*[4] do not calculate for the Seebeck coefficient, but they solve the equations for thermoelectric current density. They show that the thermoelectric current density at zero bias can change sign under special conditions that are very similar to the situation in the intuitive picture of Fig. 1. They explain that this sign change in current density should be reflected in thermopower as well.

The theoretical approach presented in this paper is different from the above references. Hence, we end up with different results, which we will explain at the end of this section.

The transport theory used in this section is based on the model presented in Ref. 2. The conductivity and Seebeck coefficient can be calculated from the number of electrons participating in transport (n_e) and the energy transported by these electrons (n_Q) respectively,

$$n_e(V) = \frac{1}{4\pi^3}\left[\frac{L_w}{L_p}\int_{-\infty}^{\infty} dk_z \frac{\hbar^2 k_z^2}{m_w^*}\int_{-\infty}^{\infty} dk_x \times \int_{-\infty}^{\infty} dk_y \left(-\frac{\partial f(k_x,k_y,k_z,E_f)}{\partial E}\right) T(k_z,V) + \frac{L_b}{L_p}\int_{-\infty}^{\infty} dk_z \frac{\hbar^2 k_z^2}{m_b^*}\int_{-\infty}^{\infty} dk_x \times \int_{-\infty}^{\infty} dk_y \left(-\frac{\partial f(k_x,k_y,k_z,E_f-E_b)}{\partial E}\right) T\left(\sqrt{k_z^2+k_b^2},V\right)\right], \tag{4}$$

where V is the applied voltage. The transmission probability (T) depends only on V and the k_{z_i} value since we have assumed that the transverse momentum is conserved. The first and second integrals are the number of transmitted electrons from the well and barrier regions respectively. The two integrals are different in their reference of energy ($E_b = \hbar^2 k_b^2 / 2m_b^*$) and the carrier's effective mass. We are considering miniband widths comparable with thermal energy. Thus we have used a bulk-type Boltzmann transport equation with a Fermi window factor of $(-\partial f/\partial E)$ and a correction due to the quantum mechanical transmission through the barrier. The energy transported by the electrons shall be calculated using the following quantity:

$$n_Q(V) = \frac{1}{4\pi^3}\left[\frac{L_w}{L_p} \times \int_{-\infty}^{\infty} dk_z \frac{\hbar^2 k_z^2}{m_w^*}\int_{-\infty}^{\infty} dk_x \int_{-\infty}^{\infty} dk_y \frac{\hbar^2}{2m_w^*}(k_x^2 + k_y^2 + k_z^2 - k_f^2)\left(-\frac{\partial f(k_x,k_y,k_z,E_f)}{\partial E}\right) T(k_z,V) + \frac{L_b}{L_p} \times \int_{-\infty}^{\infty} dk_z \frac{\hbar^2 k_z^2}{m_b^*}\int_{-\infty}^{\infty} dk_x \int_{-\infty}^{\infty} dk_y \frac{\hbar^2}{2m_b^*}(k_x^2 + k_y^2 + k_z^2 - k_f^2)\left(-\frac{\partial f(k_x,k_y,k_z,E_f-E_b)}{\partial E}\right) T\left(\sqrt{k_z^2+k_b^2},V\right)\right]. \tag{5}$$

Equation (5) is similar to Eq. (4) except that the integrand is multiplied by the difference of the energy of emitted electrons from the Fermi level. Also a dispersion relation for an electron's wave vector in the z direction is assumed, similar to the one on the xy plane. This approximation simplifies the integrations while not noticeably affecting the final results. We thus calculate the conductivity from $\sigma = en_e\mu$, and the Seebeck coefficient from $S = n_Q/en_eT$, where e, μ, and T are the electron's charge, mobility, and temperature respectively. This equation for the Seebeck coefficient is a good approximation compared to the more accurate definition $S = J_Q/TJ$, where J_Q is the heat current transported and J is the electrical current. This is because mobility in the miniband transport regime is a much weaker function of electron energy than the

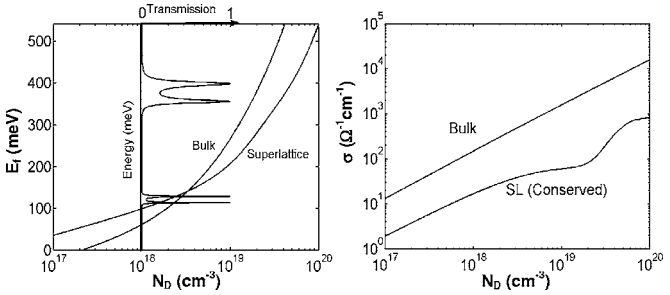

FIG. 2. Calculated Fermi energy (left) and electrical conductivity (right) vs doping concentration for InGaAs bulk and InGaAs/InAlAs superlattice. Inset shows the transmission probability of the superlattice vs energy. The scale of the energy axis is set the same as that of the Fermi energy axis for comparison.

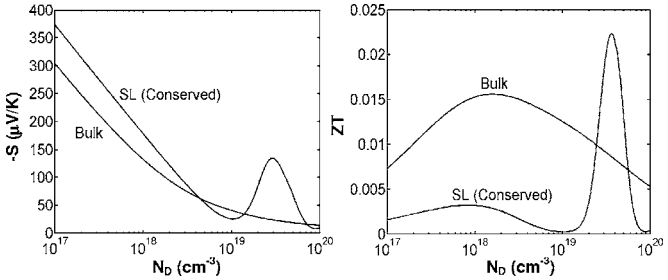

FIG. 3. Seebeck coefficient (left) and thermoelectric figure of merit (right) vs doping concentration for bulk InGaAs material and the InGaAs/InAlAs superlattice.

quantum mechanical transmission probability in superlattices. In analogy with bulk thermoelectrics, one can define the thermionic figure of merit as $ZT=\sigma S^2T/\beta$, where β is the thermal conductivity of the material. Figure 2 shows the calculated Fermi energy and electrical conductivity versus doping concentration for an InGaAs/InAlAs superlattice. For comparison, transmission probability versus energy is also illustrated on the same plot as well as the Fermi energy. Parameters used in the simulations are listed in Table I. In this table, n_w is the number of superlattice periods, L_w and L_b are the widths of well and barrier, respectively, m^* is the electron's effective mass, and α is the nonparabolicity of the conduction band. For comparison, corresponding quantities are also calculated and plotted for bulk InGaAs material. It can be seen that superlattice conductivity is about an order of magnitude smaller than that of the bulk material in the range of doping concentration. This is basically due to the fact that electronic transport happens dominantly through the two available minibands below the barrier height (E_b =450 meV).

Figure 3 shows the calculated Seebeck coefficient and thermoelectric figure of merit versus doping concentration for this structure.

Based on Fig. 1, we may have expected a change of sign for the Seebeck coefficient as the doping increases and Fermi level moves above the first miniband. However, this is not the case. Seebeck coefficient reduces significantly to about 25 μV/K at a doping of 1×10^{19} cm^{-3}. This reduction in the Seebeck coefficient happens for the second miniband too. The right-hand side of Fig. 3 shows that the maximum value of the thermoelectric figure of merit, ZT, in an InGaAs/InAlAs superlattice is slightly larger than the bulk InGaAs. This is due to the reduced electrical conductivity of the superlattices, although the superlattice's Seebeck coefficient is mostly above that of bulk materials in the whole range of doping concentrations.

Contrary to the results of Ref. 4, the sign of Seebeck coefficient *does not* change for any value of doping concentration in Fig. 3. The sign change is in fact due to two key assumptions made in Ref. 4: (i) Electron transport in superlattice minibands is in the nonlinear regime, and (ii) transmission probability does not depend on the electron's transverse kinetic energy, which implies the transverse momentum of electrons is conserved. The former assumption is true only for electron transport in *narrow* minibands (in the range of a few meV). When miniband widths are small compared to the broadening of the energy levels due to scattering or compared to the voltage drop per superlattice period, the linear miniband transport no longer exists.[5] Superlattice minibands for our existing structure are too *wide* to yield such a thermopower anomaly. In consequence, formalism of Ref. 4 is not able to explain the experimental data. In the applications in which the superlattice miniband is wide, nonlinear transport equations must be replaced with a better approximation based on linear transport theory. Our approach in this paper is based on the latter assumption and thus can explain the experimental results.[2] Although there is still thermopower anomaly seen in the left-hand side of Fig. 3, the sign of the Seebeck coefficient does not change. As we will see in the next section, the sign change in Seebeck coefficient at the given temperature may only happen if the transverse momentum of electrons is not conserved.

Cantrell *et al.*[3] have also shown that the Seebeck sign change happens only below relatively low temperatures (~10 K). Their analysis is valid when there are no sharp variations in density of states within the thermal energy, k_BT, of the Fermi level. Consequently, it does not include the effect of discontinuities such as the subband edge or other neighboring minibands. This is more likely to happen at higher temperatures. The formalism presented hereby self-consistently includes such deviations [see Eqs. (4) and (5)]. Cantrell *et al.* also derived a rather simplified expression for the highest temperature at which the Seebeck coefficient changes sign. This expression depends on the electron differential conductivity near the subband minimum. However, in

TABLE I. Structural parameters for the $In_{0.53}Ga_{0.47}As/In_{0.52}Al_{0.48}As$ superlattice (Refs. 6 and 7).

n_w	L_w (nm)	L_b (nm)	E_b (meV)	m_w^*	m_b^*	α_w (ev^{-1})	α_b (ev^{-1})	μ_w (cm^2/Vs)	μ_b (cm^2/Vs)	V_s (cm/s)
250	50	30	450	0.041	0.084	1.167	1.167	1000	6000	10^7

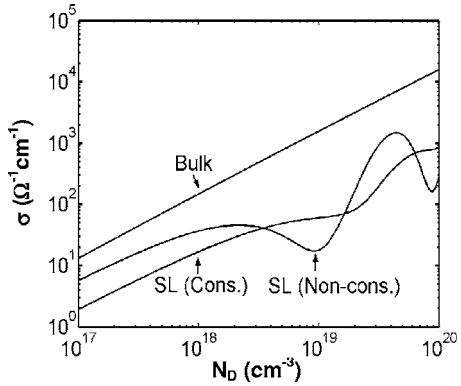

FIG. 4. Electrical conductivity (right) vs doping concentration for InGaAs bulk and InGaAs/InAlAs superlattice for two cases of conserved and nonconserved transverse momentum.

their calculation of the differential conductivity $\sigma(E)$, which is presented elsewhere,[8] the transverse momentum remains conserved.

In the following section, we will see that nonconservation of electron's transverse momentum in the thermionic current has two effects: it significantly increases thermionic figure of merit *ZT*, and it can change the sign of Seebeck coefficient for the superlattice structure under test. In Sec. IV, we present experimental results for thermoelectric transport in superlattice structures in miniband conduction regime.

III. NONCONSERVATION OF TRANSVERSE MOMENTUM

Equations (4) and (5) imply that the transmission probability $T(k_z)$ depends on the quantized energy levels inside the wells (see Ref. 2 for more details). However, when the transverse momentum is not conserved during thermionic emission, the transmission probability depends on the total energy of the electron, and not just the kinetic energy perpendicular to the well. Nonconservation of transverse momentum happens due to the interaction of the quantized charge carriers in the quantum well, both with each other and with inhomogeneities. One thus replaces $T(k_z,V)$ with $T(k_x,k_y,k_z,V)$ in Eqs. (4) and (5),

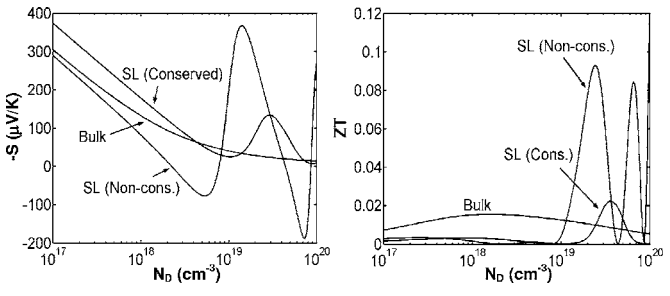

FIG. 5. Seebeck coefficient (left) and thermoelectric figure of merit (right) vs doping concentration for InGaAs bulk and InGaAs/InAlAs superlattice for two cases of conserved and nonconserved transverse momentum.

$$n_e(V) = \frac{1}{4\pi^3}\left[\frac{L_w}{L_p}\int_{-\infty}^{\infty} dk_z \frac{\hbar^2 k_z^2}{m_w^*}\int_{-\infty}^{\infty} dk_x \times \int_{-\infty}^{\infty} dk_y \left(-\frac{\partial f(k_x,k_y,k_z,E_f)}{\partial E}\right) T(k_x,k_y,k_z,V) + \frac{L_b}{L_p}\int_{-\infty}^{\infty} dk_z \frac{\hbar^2 k_z^2}{m_b^*}\int_{-\infty}^{\infty} dk_x \times \int_{-\infty}^{\infty} dk_y \left(-\frac{\partial f(k_x,k_y,k_z,E_f - E_b)}{\partial E}\right) T(k_x,k_y,\sqrt{k_z^2+k_b^2},V)\right]. \quad (6)$$

For thermionic power, we calculate the following integral when the transverse momentum is not conserved:

$$n_Q(V) = \frac{1}{4\pi^3}\left[\frac{L_w}{L_p} \times \int_{-\infty}^{\infty} dk_z \frac{\hbar^2 k_z^2}{m_w^*}\int_{-\infty}^{\infty} dk_x \int_{-\infty}^{\infty} dk_y \frac{\hbar^2}{2m_w^*}(k_x^2 + k_y^2 + k_z^2 - k_f^2)\left(-\frac{\partial f(k_x,k_y,k_z,E_f)}{\partial E}\right) T(k_x,k_y,k_z,V) + \frac{L_b}{L_p} \times \int_{-\infty}^{\infty} dk_z \frac{\hbar^2 k_z^2}{m_b^*}\int_{-\infty}^{\infty} dk_x \int_{-\infty}^{\infty} dk_y \frac{\hbar^2}{2m_b^*}(k_x^2 + k_y^2 + k_z^2 - k_f^2)\left(-\frac{\partial f(k_x,k_y,k_z,E_f - E_b)}{\partial E}\right) \times T(k_x,k_y,\sqrt{k_z^2+k_b^2},V)\right]. \quad (7)$$

Figure 4 shows the conductivity of the same structure with the assumption that transverse momentum is not conserved.

It is seen that when the transverse momentum is not conserved, the electrical conductivity of the superlattice can be three times larger than the value for the conserved transverse momentum case at some doping concentrations. Figure 5 shows the corresponding Seebeck coefficient and thermoelectric figure of merit. It can be seen that the Seebeck coefficient changes sign when the Fermi energy is close to the minibands (see the left-hand side of Fig. 2). Positive Seebeck coefficient peaks of about 100 μV/K and 200 μV/K are predicted at a doping of 5×10^{18} cm^{-3} and 7×10^{19} cm^{-3}, respectively. Interestingly, the thermionic figure of merit for the case of nonconserved transverse momentum is about four times larger than that of the conserved transverse momentum case, and about six times larger than that of bulk. It should be noted that this improvement in *ZT* is due to the improvement in the effective power factor. This improvement can be combined with the other methods to reduce the phonon thermal conductivity in superlattices and thus obtain a higher thermoelectric figure of merit.[9–11]

Surprisingly, Fig. 4 shows that the electrical conductivity for the case of conserved transverse momentum can be larger than that of nonconserved transverse momentum at some doping levels. This is counterintuitive; we would expect the

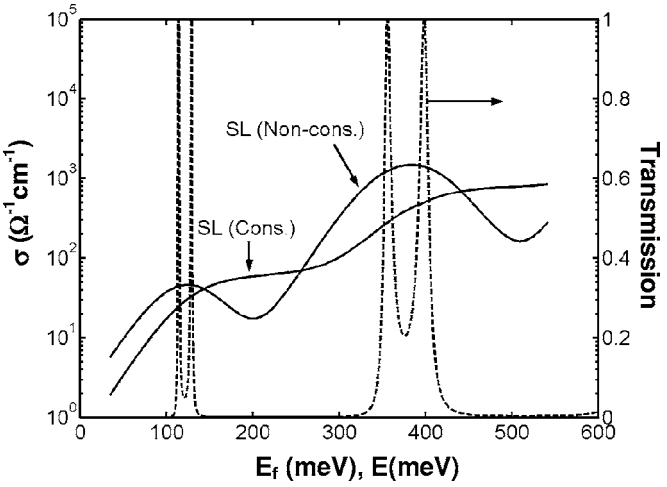

FIG. 6. Electrical conductivity vs Fermi energy (left axis), and transmission probability vs energy (right axis) for two cases of conserved and nonconserved transverse momentum.

nonconservation of transverse momentum to increase number of electrons tunneling through the barrier.[12] We devote a paragraph clarifying this discrepancy.

Figure 6 shows electrical conductivity versus Fermi energy for the two cases of conserved and nonconserved transverse momentum. The corresponding transmission probability versus energy is also plotted on the same x axis for comparison. It is noted in this figure that when the transverse momentum is conserved, the electrical conductivity rises rapidly when the Fermi energy is within the minibands and slowly when it is far from the minibands. However, when the transverse momentum is not conserved, the electrical conductivity has peaks when Fermi energy lies within the minibands, and decreases below that of the conserved transverse momentum case when it moves out of the miniband. The unexpected electrical conductivity of Fig. 6 can be best understood from the momentum space diagram of the left-hand side of Fig. 7. This figure depicts the Fermi sphere and a quantized energy surface in k space. For simplicity we consider a single energy state, but the conclusion is equally valid for the case of minibands. Transport takes place within the thermally spread states around the Fermi surface (E

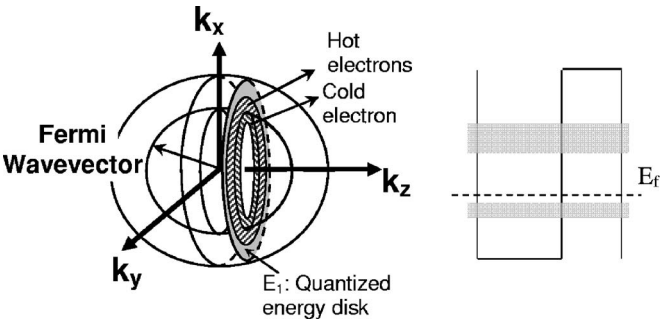

FIG. 7. Left: Transverse momentum conserved; most of the electrons in the first miniband are above Fermi energy (Seebeck coefficient negative). Right: transverse momentum not conserved; most of the electrons move below Fermi energy (Seebeck coefficient positive).

$\sim E_f \pm k_B T$). When the transverse momentum is conserved, transmission probability depends only on k_z (the electron's wave vector perpendicular to the superlattice layer), thus quantized energy levels make flat surfaces in k space as shown on the left in Fig. 7. States participating in the transport are the ones in the overlap area of the thermally spread states around the Fermi surface and the quantized energy surface. For the case of conserved transverse momentum, when the Fermi energy is about at the energy of the first quantized energy level, electrical conductivity increases with the Fermi energy due to the increase of the overlap area. However, when the Fermi energy is larger than the quantized energy level, the overlap area, and thus the electrical conductivity, does not change very noticeably. The electrical conductivity increases again as the Fermi energy increases to the level of the second quantized energy surface. With a similar perspective, we can explain why the Seebeck coefficient never changes sign in the left-hand side of Fig. 3 when the transverse momentum is conserved. This is because in the quantized energy disk, the number of hot electrons with energies above the Fermi level is always more than that below the Fermi level (cold electrons) (see the left-hand side of Fig. 7).

On the other hand, nonconservation of transverse momentum can affect the structure of the minibands. Minibands are formed as a result of the additional periodicity of the superlattice in the growth direction. In the in-plane direction, there is no periodic structure and electrons are not expected to be affected by minibands. However, if due to scatterings, the electron transverse momentum is not conserved, the transmission probability depends on the total energy, and minibands are no longer flat bands in k space. At the extreme point that the transverse momentum is not conserved for all electrons, one may use the transmission probability in the growth direction and then replace k_z by k, as in Eqs. (6) and (7). This approximation is effectively equal to an assumption of the formation of spherical minibands. This model is an approximate way to take into account nonconservation of transverse momentum and a more detailed analysis of this effect is needed. In the case of a spherical miniband described by Eqs. (6) and (7), when the Fermi energy is within a miniband, the volume of the overlap states between the thermally spread states around the Fermi level and the miniband reaches its maximum and a peak appears in the electrical conductivity as seen in Fig. 6. However, when the Fermi energy is out of the miniband, the overlap volume vanishes (or only the tail of the Fermi sphere is left in the minibands), thus the electrical conductivity decreases significantly.

In the next section we discuss experiments investigating the cross-plane Seebeck coefficient of superlattice structures in miniband conduction regime.

IV. EXPERIMENTS

The molecular beam epitaxy (MBE) grown superlattice contained 25 periods of 5-nm thick InGaAs n-doped with varying concentrations, 2×10^{18}, 4×10^{18}, 8×10^{18}, to 3 $\times10^{19}$ cm^{-3}, and 3-nm thick undoped InAlAs. The superlattice layer composition was lattice matched to the InP sub-

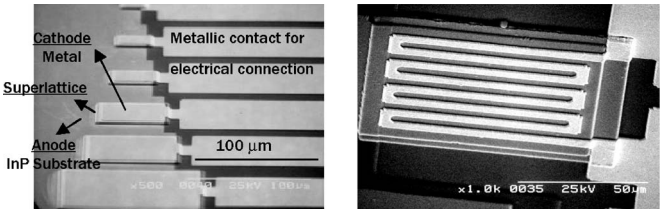

FIG. 8. A cope of the device structure (left), and the microcooler integrated with heaters (right).

strate. 0.5-μm thick highly doped (1×10^{19} cm^{-3}) InGaAs layers were used as the buffer and the cap layers. These facilitate contact metallization on top and on the bottom of the superlattice. Devices with various sizes were fabricated using conventional lithography, dry etching, and metallization techniques. Ni/AuGe/Ni/Au was used to make ohmic contacts to both electrodes. The left side of Fig. 8 shows the device's geometry under the scanning electron microscope (SEM). A thin film heater was deposited on top of the microcooler and used as both heat source and temperature sensor, as illustrated in the right-hand side of Fig. 8.

At last, the sample was attached to a package, wire bonded, and loaded into the cryostat. There were a total of four samples under test with different dopings in the superlattice layer. We used two device sizes, 100×100 μm^2 and 70×70 μm^2, for measurements. First, we calibrated the heater resistance with the stage temperature. We used four-wire measurement to measure the resistance to reduce the influence of contact wires and pads. At a given heater power, the top of the cooler device was heated up by the thin film heater at a fixed temperature (T_h). The substrate was attached to the heatsink inside the cryostat, where the temperature was controlled by the flow of liquid Helium (T_s). The temperature difference across the superlattice layer ($\Delta T=T_h-T_s$) generates a voltage difference (ΔV), which can be measured by probing the microcooler contact and ground contact. Thus, the effective Seebeck coefficient of the device could be calculated easily from $S=\Delta V/\Delta T$. ΔV is voltage difference across the junction, and ΔT is the temperature difference across the junction. As long as we could measure the voltage and temperature difference accurately, the Seebeck coefficient could be calculated. The difficulty of characterizing the Seebeck coefficient of a superlattice thin film lies in simultaneously measuring voltage and temperature drops to within a few microns on both sides of the film. We successfully measured the Seebeck coefficient by integrating a thin film heater on top of the microcooler.[13] For the detailed calculation methods used to derive the Seebeck coefficient of the superlattice, refer to Ref. 14. The Seebeck coefficients were measured through the cryostat temperature change from 10 K to 300 K.

V. RESULTS AND SIMULATIONS

Figure 9 illustrates the measured Seebeck coefficients along with theoretical calculations for samples *A*, *B*, *C*, *D* with doping concentration ranging from 2×10^{18} to 3×10^{19} cm^{-3}. From the graph, we can see the Seebeck coefficient increases with temperature for all samples. The graph verifies that the Seebeck coefficient is independent of device size. The Seebeck coefficient measured for both 100×100 μm^2 (squares) and 70×70 μm^2 (circles) devices match except for one case. We found that the discrepancy was due to a fabrication error for the sample *D* of size 100×100 μm^2. Heater wire was shortened in a small area. For sample *D*, data for the device of size 70×70 μm^2 is used for comparison with theoretical predictions.

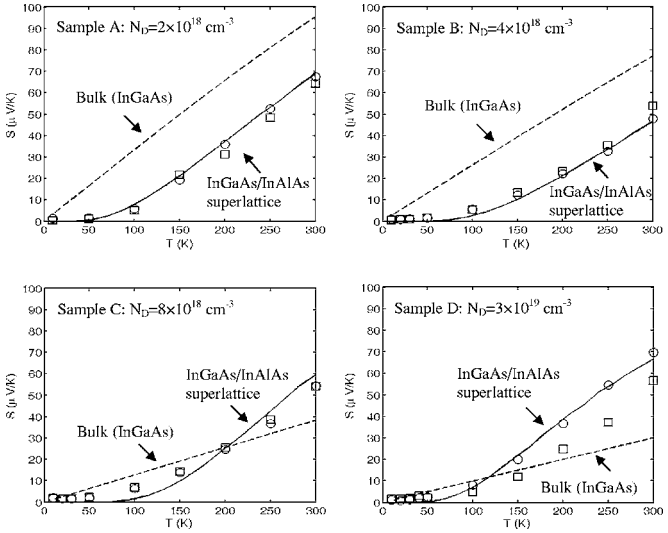

FIG. 9. The measured effective Seebeck coefficient for samples *A*, *B*, *C*, *D*. Circles (device size 70×70 μm^2) and squares (device size 100×100 μm^2) are experimental data, the lines are theoretical modeling.

The theoretical fitting was based on the model presented in Sec. II, which assumes that the transverse momentum is conserved. The transmission probability is calculated with the use of the transfer matrix method (TMM). Since the resulting minibands' widths are either on the order of, or larger than, the thermal energy (~20 meV and 100 meV for the first two minibands), a bulk-type Boltzmann transport with a correction accounting for quantum mechanical transmission above and below the barrier is assumed [Eqs. (4) and (5)]. Parameters used in the calculations are listed in Table I.[15]

The left-hand side of Fig. 10 illustrates the superlattice transmission coefficient as a function of electron energy. Given the finite coherence length of carriers, only two periods are taken into account. Three minibands at approximately 120, 380, and 670 meV can be identified. The positions of Fermi levels for the four samples are also shown. The right-hand side of Fig. 10 illustrates the theoretical prediction of the Seebeck coefficient as a function of doping concentration, along with the experimental data points (circles and squares). From the graph, we can see that the Seebeck coefficient monotonically decreases with doping concentrations up to 10^{19} cm^{-3}, but it starts to increase with the doping concentration. This trend was confirmed by the increased Seebeck coefficient measured for sample *D*. As it can be seen in Fig. 9, sample *D*'s Seebeck coefficient is lager than bulk InGaAs doped at the same level, while the Seebeck coefficients of samples *A*, *B*, and *C* were lower than bulk values over the whole temperature range. The Seebeck coef-

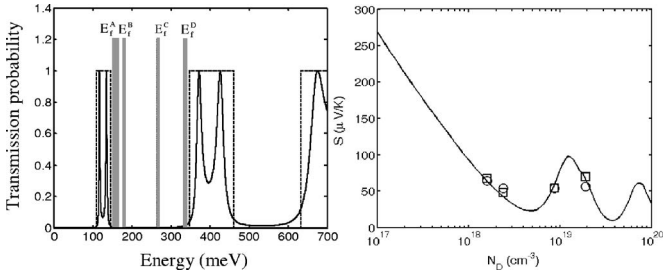

FIG. 10. Left: Superlattice transmission coefficients vs energy calculated with the use of TMM (solid line) and Kronig-Penney model (dashed line). Positions of Fermi levels for samples *A*, *B*, *C*, and *D* are also indicated. Right: The theoretical Seebeck coefficient as a function of doping concentration along with the measured data for the four samples.

ficient of samples *A*, *B*, and *D* fit the theoretical calculations for well and barrier widths of 43 and 30 Å, respectively. However, sample *C* is well fitted with the well and barrier widths of 50 and 30 Å, respectively. This variation could be due to different growth rates between epitaxial growths. The thickness variations were verified by measuring the superlattice period accurately with the use of x-ray diffraction.

VI. SUMMARY

We described detailed calculation of thermoelectric effects in short period superlattice devices. Nonmonotonic behavior of the cross-plane Seebeck coefficient versus doping was observed. This was explained due to miniband conduction regime. Simple diagram shown in Fig. 1 suggests that the sign of the Seebeck coefficient could be changed compared to that of bulk *n*-doped material. However, we did not observe the sign change experimentally. When we carefully examined the theoretical model, we found out that only when the electron's transverse momentum is not conserved during quantum mechanical transmission the sign of the Seebeck coefficient could be changed (see Fig. 5). Transverse momentum conservation is a consequence of translational symmetry in the plane of quantum wells, and it could be violated by adding any substructure that breaks this symmetry such as embedded quantum dots. Calculations in Ref. 16 illustrated indeed the Seebeck coefficient sign change as *p*-doping increases for Ge/Si quantum dots superlattices. In the case of planar barrier, when transverse momentum is conserved, sign of the Seebeck coefficient does not change and we only see a nonmonotonic variation of the Seebeck coefficient versus doping.

ACKNOWLEDGMENTS

This work was supported by the MURI TEC Center program and the Packard Foundation.

*Electronic address: daryoosh@soe.ucsc.edu

[1] D. Vashaee and A. Shakouri, Phys. Rev. Lett. **92**, 106103-1 (2004).
[2] D. Vashaee and A. Shakouri, J. Appl. Phys. **95**, 1233, (2004).
[3] D. G. Cantrell and P. N. Butcher, J. Phys. C **18**, L587 (1985).
[4] Magnus Larsson, Vadim B. Antonyuk, A. G. Mal'shukov, and K. A. Chao, Phys. Rev. B **68**, 233302 (2003).
[5] Luis L. Bonilla and Holger T Grahn, Rep. Prog. Phys. **68**, 577 (2005).
[6] R. People, K. W. Wecht, K. Alavi, and A. Y. Cho, Appl. Phys. Lett. **43**, 118 (1983).
[7] An average effective mass of $0.05m_e$ is assumed in Eqs. (4)–(7).
[8] D. G. Cantrell and P. N. Butcher, J. Phys. C **18**, 5111 (1985).
[9] G. Chen, Semicond. Semimetals **71**, 203 (2001).
[10] R. Venkatasubramanian, Semicond. Semimetals **71**, 175 (2001).
[11] R. Venkatasubramanian, E. Siivola, T. Colpitts, and B. O'Quinn, Nature **413**, 597 (2001).
[12] S. V. Meshkov, Sov. Phys. JETP **64**, 1337 (1986).
[13] Y. Zhang, G. Zeng, R. Singh, J. Christofferson, E. Croke, J. E. Bowers, and A. Shakouri, "*Measurement of Seebeck coefficient perpendicular to* SiGe *superlattice layers*," 21st International Conference on Thermoelectrics, Long Beach CA, 26-29 August 2002.
[14] G. Chen, Phys. Rev. B **57**, 14958 (1998).
[15] Doping concentrations were determined to be 1.6×10^{18}, 2.4×10^{18}, 8.7×10^{18}, and 1.4×10^{19} cm^{-3} to fit the experimental data of samples *A*, *B*, *C*, and *D* respectively. For all samples, it is assumed that only wells are doped.
[16] Alexander A. Balandin and Olga L. Lazarenkova, Appl. Phys. Lett. **82**, P415 (2003).